Alignment and orientation of the excited H(2p) orbital following H + He collisions at intermediate energies

M. Kimura
Argonne National Laboratory, Argonne, Illinois 60439
and Department of Physics, Rice University, Houston, Texas 77251

N. F. Lane
Department of Physics, Rice University and Rice Quantum Institute, Houston, Texas 77251
(Received 23 September 1987)

A systematic theoretical study of alignment and orientation of the excited H(2p) orbital in H + He collisions in the energy range from 0.8 to 8 keV is carried out with use of a molecular-orbital representation. The present model takes the active electron in the H atom explicitly into account, while treating the He atom as a frozen core. Calculated alignment and orientation agree very well with recent measurements, implying that the dominant excitation mechanism for H(2p) excitation is the strong $X\,^2\Sigma - A\,^2\Sigma$ radial coupling for all energies studied. Hence, the integral alignment A_{20} is negative and slowly varying with energy. Present partial excitation cross sections for H(2s) and H(2p) agree well with the corresponding measurements, except at energies below 1–2 keV.

I. INTRODUCTION

Only recently has it been possible to carry out detailed experimental and theoretical studies of alignment and orientation of electronic charge clouds of atoms resulting from excitation or charge transfer during ion-atom collision processes.[1] Such studies provide deeper insight into our understanding of excitation and charge-transfer collision dynamics in heavy-particle collisions than does the simple determination of probabilities or cross sections for the same processes. However, an accurate determination or extraction of orientation and alignment parameters from either experiment or theory requires very careful treatment, since these parameters are extremely sensitive to any of the collision parameters.

Although there exist some theoretical studies of many-electron systems including $H^+ + He$ (Refs. 2 and 3) and $Li^+ + He$,[4] most alignment and orientation studies have been concentrated on one-electron or quasi-one-electron systems,[5] i.e., collision systems characterized by the presence of a one-valence electron outside two tight cores. These one-electron and quasi-one-electron systems could provide the more decisive tests of the theory. Unfortunately, there have been no fully satisfactory theoretical efforts to treat these one-electron systems until the very recent results for excitation of the Na(3p) state by proton impact obtained by Fritsch,[6] who used the so-called "AO + method."

Very interesting experiments on the determination of polarization parameters for H + rare-gas collisions have been carried out by Hippler *et al.*[7] These measurements appear to offer information that will help with our understanding of the important excitation mechanisms in the general case of atomic collisions involving rare-gas atoms. We have conducted a systematic study of the alignment and orientation of excited H(2p) orbitals resulting from H + He collisions using a molecular-orbital representation in the energy regime from 0.8 to 8 keV. The two electrons in the He atom are tightly bound and, hence, are only slightly influenced during the collision for these collision energies. It is felt to be a good approximation to assume that only the electron in the H atom is actively involved in the actual collision dynamics. Our theoretical model takes advantage of this simplification in obtaining the molecular states of this system.

II. THEORETICAL MODEL

For the purpose of simplifying subsequent related publications, we will discuss the theoretical approach in some detail in this paper.

A. Molecular state

One-electron, configuration-interaction (CI) structural calculations were carried out in order to obtain the molecular wave functions and energies. Pseudopotentials[8] were used to represent the inactive electrons. Within the Born-Oppenheimer approximation, the calculation of the eigenvalues reduces to determining the solution of the one-electron Schrödinger equation (atomic units are used throughout)

$$[-\tfrac{1}{2}\nabla_r^2 + V_A(\mathbf{r}_A) + V_B(\mathbf{r}_B) + V_{CT}(\mathbf{r}_B,R) + V_{AB}(R) - E_i(R)]\phi_i(\mathbf{r},R) = 0 , \quad (1)$$

where $\mathbf{r}_A$ is the position vector of the single active electron with respect to the A atom and $\mathbf{r}_B$ represents the electron with respect to the B atom. Correspondingly, $V_A(\mathbf{r}_A)$ and $V_B(\mathbf{r}_B)$ are the effective interactive potentials between the electron and the A core and the B atom, respectively. The potential $V_{CT}(\mathbf{r}_B,R)$ is the three-body

interaction which arises from the polarization of the B atom by both the electron and the A atom, and $V_{AB}(R)$ is the potential that approximates the interaction between the A and B atoms.

The l-dependent pseudopotentials $V_A(\mathbf{r}_A)$ and $V_B(\mathbf{r}_B)$ for the interaction of the electron with $X=A$ or B are given in the general case by

$$V_x(\mathbf{r}_x)=\sum_{l=0}^{\infty}\sum_{m=-l}^{l} V_x(r_x)\,|\,Y_{lm}(\hat{\mathbf{r}}_x)\rangle\langle\,Y_{lm}(\hat{\mathbf{r}}_x)\,|\ , \quad (2)$$

with

$$V_x(r_x)=a_{xl}\exp(-b_{xl}r^2)-\frac{Z_x}{r_x}-\frac{\alpha_{xd}}{2(r_x^2+d_x^2)^2}-\frac{\alpha_{xq}}{2(r_x^2+d_x^2)^3}\ . \quad (3)$$

The Gaussian parameters a_l and b_l are determined by iterative fits to spectroscopic data. The parameter Z_x is the charge of the core as seen by the electron at large distances, and α_d and α_q are the dipole and quadrupole polarizabilities, respectively. The quadrupole polarizability for the He atom also includes a dynamical correction term -6β ($\beta=0.706$).[9] The cross term $V_{CT}(\mathbf{r}_B,R)$ has been defined previously,[9] and was incorporated in order to have the correct behavior of the adiabatic potentials at large internuclear distances.

The pseudopotential parameters for He are given in Table I. These values were taken from the work of Pascale.[9] The cutoff parameter d serves to limit the range of the dipole and quadrupole forces to the region outside the core.

The Slater-type orbital basis sets centered on the H atom were employed in the calculations. Of importance for the scattering calculations was the reproducibility of the atomic energy splittings, which are found to agree with spectroscopic values to better than 1 meV for H. Spin-orbit effects were not included in the calculations.

B. Coupled equations

Assuming that the nuclear motion is described classically by $R(t)$, we solved the resulting time-dependent Schrödinger equation for the electron. The state vector is expanded in an electron-translation-factor (ETF) modified-molecular-state basis,[10]

$$\psi(\mathbf{r},t)=\sum_i a_i(t)\phi_i^{MO}(\mathbf{r},R(t))\exp\left[\frac{i}{2}\mathbf{v}\cdot\mathbf{r}f_n(\mathbf{r},R)\right]\ , \quad (4)$$

where $f_n(\mathbf{r},R)$ is the switching function, which is required to approach ±1 asymptotically ($R\to\infty$), depending upon the site to which an electron attaches itself.[10] Note that the ϕ_i^{MO}'s are the usual Born-Oppenheimer states, which satisfy Eq. (1), and which are obtained by the method described in Sec. II A. Substitution of Eq. (4) into the time-dependent Schrödinger equation yields the first-order, linear, coupled equations, according to the standard procedure[11]

$$i\dot{a}_i=E_ia_i+\sum_j \mathbf{v}\cdot(\mathbf{P}+\mathbf{A})_{ij}a_j\ , \quad (5)$$

where

$$P_{ij}=\langle\phi_i\,|\,-i\nabla_R\,|\,\phi_j\rangle\ , \quad (6a)$$

$$A_{ij}=i\langle\phi_i\,|\,[H_{el},\tfrac{1}{2}f_j\mathbf{r}]\,|\,\phi_j\rangle\ . \quad (6b)$$

The matrix element P_{ij} is designated as the nonadiabatic coupling, and A_{ij} represents the ETF correction. We have adopted a switching function of the form

$$f_i(\mathbf{r},R)=\tanh(R\beta_i\eta)\ , \quad (7)$$

where β_i is a parameter and η is the "angular" spheroidal coordinate. The parameter β_i was determined to minimize the sum of the square of the ETF-corrected nonadiabatic coupling matrix elements to $H(n=4)$ excited states.[11] In a rotating coordinate frame, Eqs. (6a) and (6b) are made up of two distinct contributions, namely, radial and rotational coupling and their corresponding ETF corrections. Equations (5) are solved numerically to obtain the scattering amplitude for various channels, subject to appropriate initial condition. The square of the scattering amplitude gives the transition probability for a selected channel of interest at a specific collision energy and impact parameter. Straight-line trajectories were employed for the heavy particles.

C. Polarization parameters

Briefly, the alignment angle γ and angular momentum (orientation) $\langle L_\perp\rangle$ for the electron cloud for the ^2P state are defined in terms of three Stokes parameters (P_1,P_2,P_3) [Refs. 1(a) and 12] as

$$\tan(2\gamma)=\frac{P_2}{P_1} \quad (8a)$$

and

$$\langle L_\perp\rangle=-\frac{P_3}{P}\ . \quad (8b)$$

The Stokes parameters are defined as

$$P_1=2\lambda-1\ , \quad (9a)$$

$$P_2=-2\sqrt{\lambda(1-\lambda)}\cos\chi\ , \quad (9b)$$

TABLE I. Pseudopotential parameters (in a.u.).

	He
a_0	+2.030
a_1	−1.000
a_2	
b_0	+0.463
b_1	+1.000
b_2	
q	+0.0
d	1.00
α_d	1.3834
α_q	0.8573

$$P_3 = 2\sqrt{\lambda(1-\lambda)}\sin\chi \ , \tag{9c}$$

$$P = P_1 + P_2 + P_3 \ , \tag{9d}$$

where

$$\lambda = \frac{|a_\sigma|^2}{|a_\sigma|^2 + |a_\pi|^2} \ , \tag{10a}$$

$$\chi = \arg\left|\frac{a_\pi}{a_\sigma}\right| \ , \tag{10b}$$

where a_σ and a_π are the σ and π state amplitudes, respectively. The integral alignment A_{20} is defined as

$$A_{20} = \frac{\sigma_1 - \sigma_0}{\sigma_0 + 2\sigma_1} \ ,$$

where σ_1 and σ_0 are the m-substate cross sections for $H(2p_{\pm 1})$ and $H(2p_0)$ excitation, respectively. (See Ref. 12 for details.)

III. RESULTS AND DISCUSSIONS

We have carried out seven-state [H(1s), H(2s), H(2p_0), $H(2p_\pm)$, H(3s), H(3p_0), and H(3$p_{\pm 1}$)] close-coupling calculations to obtain the excitation amplitudes by solving Eqs. (5) for collision energies in the range 0.8 to 8 keV. From these amplitudes, all polarization parameters, as well as partial cross sections, were determined and will be reported in the following paragraph.

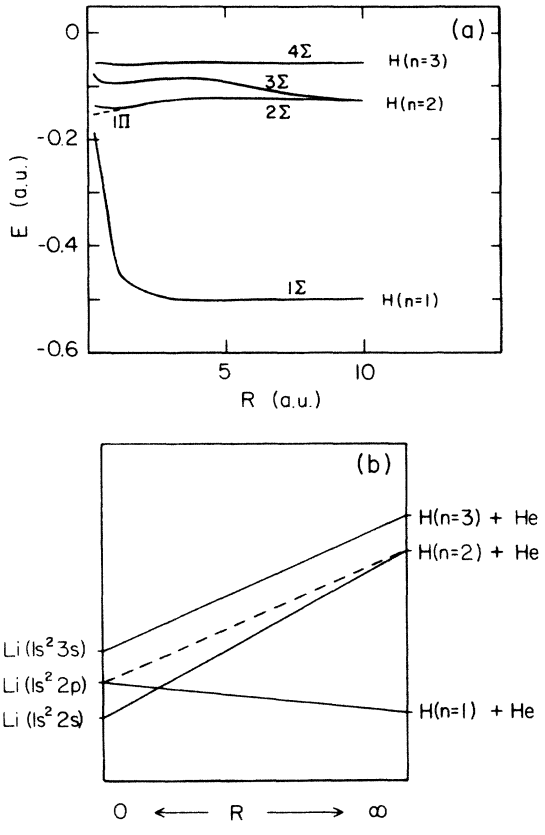

FIG. 1. (a) Adiabatic potentials for the HHe system. Solid line: Σ state; dashed line: Π state. (b) Schematic molecular correlation diagram of the HHe system.

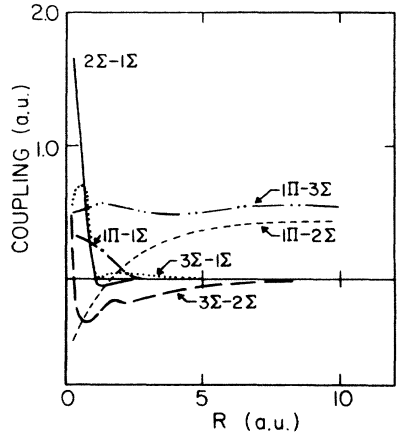

FIG. 2. Important radial and rotational couplings.

(i) *Adiabatic potentials and coupling matrix elements.* The adiabatic potential energies for the HeH system are displayed in Fig. 1(a). The $^2\Sigma$ (solid lines) and the $^2\Pi$ (dashed lines) molecular states are shown. The schematic molecular correlation diagram of the system is also shown in Fig. 1(b).

A general feature of the potential energies is the occurrence of strong configuration mixing between the 1Σ and 2Σ molecular configurations at $R \lesssim 0.5a_0$. This is because the 1Σ and 2Σ correlate to Li($1s^2 2p$) and Li($1s^2 2s$) atomic states at the united atom limit as seen in Fig. 1(b). This curve crossing at $R \simeq 0.5a_0$ plays a significant role in causing flux promotion during the incoming part of the collision. However, flux given to the 2Σ configuration will be redistributed by additional strong radial and rotational couplings within the H($n=2$) manifold. The 1Σ and 1Π configurations are degenerate in the united atom limit, coinciding with the Li($1s^2 2p$) atomic level [see Fig. 1(b)]. Thus, one expects a relatively strong rotational coupling between these states at small R. The 2Σ and 1Π configurations are almost identical except for the small-R region ($\lesssim 1.5a_0$) and thus, outside this region, the corresponding rotational coupling might be expected to cause some flux redistribution within the H($n=2$) manifold.

The behavior exhibited by the adiabatic energy curves is borne out by the radial coupling matrix elements. The important coupling terms between the ground and H($n=2$) levels are shown in Fig. 2. The calculations indicate strong radial coupling between the 1Σ and 2Σ states that peaks at $R \approx 0.2a_0$. Other radial couplings involving the ground 1Σ state are relatively weak at all internuclear separations. The radial coupling between 2Σ and 3Σ states possesses a long-range tail extending beyond $R \simeq 5a_0$. This tail may play an important role in flux redistribution in the outgoing part of collision. The rotational coupling between the 1Σ and 1Π states is found to be of secondary importance. The close-coupled

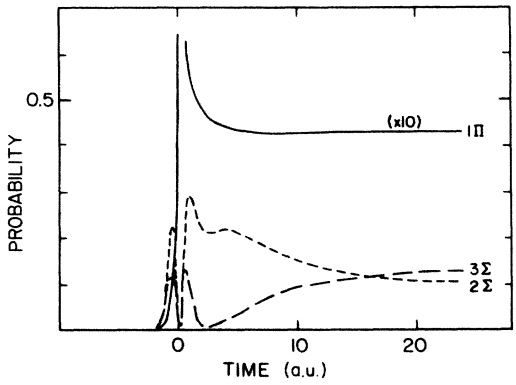

FIG. 3. Collision history excitation probabilities vs collision time at $E=4$ keV and $b=0.2$ a.u.

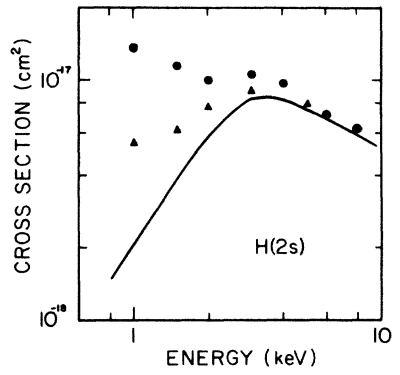

FIG. 4. H(2s) excitation cross section. ——, present; ●, Ref. 13; ▲, Ref. 14.

scattering calculations included all Σ and Π molecular states up to H($n=3$) levels, along with all possible radial and rotational coupling matrix elements between these states.

(ii) *Collision dynamics and excitation cross section.* A collision history, i.e., excitation probabilities plotted as functions of collision time, at $E=4$ keV and impact parameter $b=0.2$ a.u., is displayed in Fig. 3. As is clearly indicated, the Π state couples with the Σ states only at small R, and then completely decouples soon after. This behavior is reflected in a flat and constant probability for the Π state just beyond the classical turning point. The 2Σ and 3Σ states continue to couple with one another until quite large internuclear separations, and therefore contribute significantly to the redistribution of flux between the H(2s) and H(2p) states. As b is increased, flux promotion to the excited Π state through 1Σ-1Π rotational coupling quickly disappears, as is apparent from the coupling shown in Fig. 2. However, certain general features of the coupling scheme, namely, short-range 1Σ-1Π coupling and long-range 2Σ-1Π, 3Σ-1Π, and 2Σ-3Π coupling, remain unchanged regardless of the collision energy and impact parameter chosen. From a collision-dynamics point of view, no drastic change of coupling scheme is expected to occur in the energy range studied. Also, it should be pointed out that all probabilities fall off beyond $b\sim 3$ a.u. in the energy region studied.

Partial-excitation cross sections for the H(2s) and H(2p) states are depicted in Figs. 4 and 5, respectively, along with experimental data. For H(2s) excitation above $E\simeq 5$ keV, present theoretical results are in excellent accord with the measurements of Birely and McNeal[13] and Sauers and Thomas.[14] In the energy region from 0.8 to 5 keV, the experimental cross sections are significantly larger than our results. Moreover, one set of data, that of Birely and McNeal,[13] show a quite different energy dependence, with the cross section increasing with decreasing energy. The calculated cross section shows a peak around $E\simeq 3.5$ keV and then decreases at lower energies, a behavior that is qualitatively similar to the measurement of Sauers and Thomas.[14]

For H(2p) excitation, the present results are in good accord with experimental measurements[13,15] above ~3 keV as shown in Fig. 5. However, at lower energies we again see discrepancies between the present result and the measurements. The theoretical cross section seems to fall off rather more rapidly compared to the experimental results.

Although there exist other theoretical treatments, including the Born approximation[16] and the one-center atomic-orbital (AO) expansion method,[16–19] in the energy regime which overlaps the present study for H($n=2$) excitations, these approaches are considered not to be appropriate in this energy regime[15,20] since flux population in excited states involves the multiple-step mechanism and therefore will not be discussed further. (See Ref. 20 for detail criticism on this point.) Additional experimental studies in this energy range would be helpful to resolve these discrepancies.

(iii) *Alignment and orientation.* The present integrated (over the impact parameter) alignment A_{20} for the excited H(2p) states is shown in Fig. 6 along with the measurement by Hippler *et al.*[7] The negative values observed for A_{20} indicate that excitation to the H($2p_0$) level is the overwhelmingly dominant process; theoretically

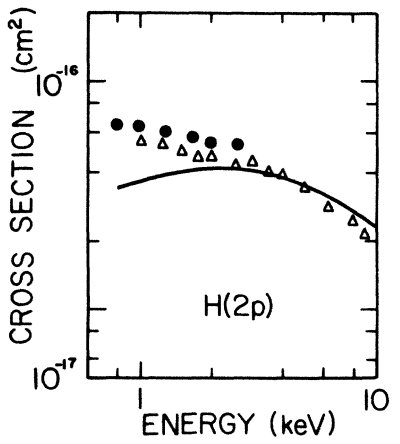

FIG. 5. H(2p) excitation cross section. ——, present; ●, Ref. 15; △, Ref. 13.

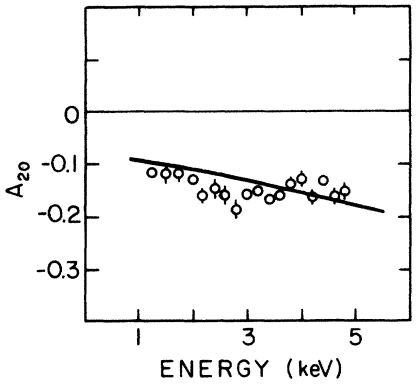

FIG. 6. Integrated (over impact parameter) alignment A_{20}. ——, present; ○, Ref. 7.

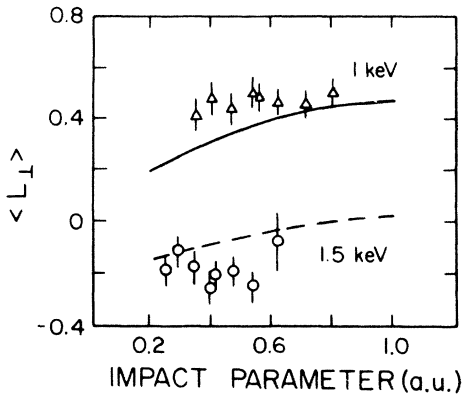

FIG. 8. Transferred angular momentum $\langle L_\perp \rangle$ at $E=1$ and 1.5 keV. —— and — — —, present; ○, △, Ref. 7.

this is found to occur through the strong 1Σ-2Σ radial coupling in this energy regime. The less prominent structure seen in the A_{20} measurements also indicates that there is very little interference from other types of coupling. From a theoretical perspective, this is clear from the collision history illustrated in Fig. 3. The small variation of A_{20} with respect to collision energy can also be explained in terms of the dominance of a single strong radial coupling. A similar energy dependence of A_{20} is also found for H on Ne and Ar target cases both experimentally[7] and theoretically.[21] Since the general nature of the adiabatic potential curves, apart from details, is qualitatively quite similar for all three systems, the observed similarity in A_{20} is not surprising.

The differential alignment A_{20} is plotted as a function of impact parameter b in Fig. 7 at $E=1$ and 1.5 keV along with the measurements of Hippler *et al.*[7] The differential alignment A_{20} clearly reveals details of the coupling scheme active in the excitation of $H(n=2)$ levels during the collision which are, to a large extent, masked in the study of the integrated (over b) alignment (see above). Below $b \simeq 1a_0$ ($0.5a_0$) for $E=1$ keV (1.5 keV), respectively, the contribution to the differential A_{20} comes predominantly from the $H(2p_0)$ sublevel due to the strong 1Σ-2Σ radial coupling. However, as the impact parameter is increased, strong rotational couplings within the $H(n=2)$ manifold, i.e., 2Σ-1Π and 3Σ-1Π coupling, became effective in promoting flux mixing among the 2Σ, 3Σ, and 1Π configurations and in giving rise to increased population of the $H(2p_{\pm 1})$ sublevel. Correspondingly, this is reflected in a pronounced impact-parameter dependence of the differential A_{20}. Although the general shapes of the differential A_{20} parameters at the two energies are relatively similar, the magnitudes are obviously different at a given impact parameter. This implies that the coupling scheme is somewhat sensitive to the collision energy.

The calculated transferred angular momentum $\langle L_\perp \rangle$ (or orientation) perpendicular to the scattering plane is depicted in Fig. 8 as a function impact parameter for the two energies 1.0 and 1.5 keV along with the experimental results of Hippler *et al.*[7] Agreement between the present theory and the experiment is reasonably good. Neither the theoretical nor the experimental curves show any notable structure except for a slightly increasing trend of the calculated angular momentum $\langle L_\perp \rangle$ at larger b, whereas

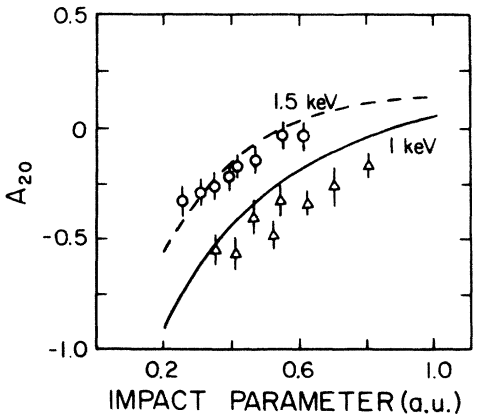

FIG. 7. Differential alignment A_{20} at $E=1$ and 1.5 keV. —— and — — — lines, present; ○, △, Ref. 7.

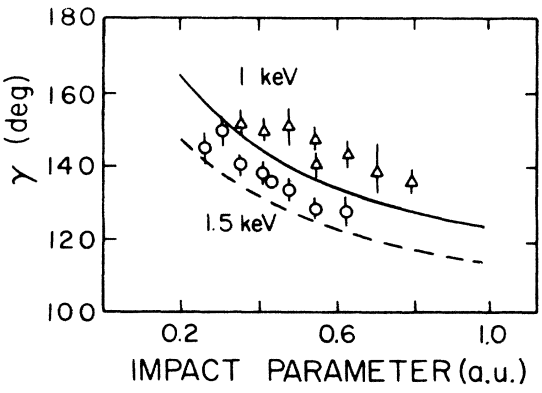

FIG. 9. Alignment angle γ at $E=1$ and 1.5 keV. —— and — — —, present; ○, △, Ref. 7.

a relatively strong energy dependence is observed. The factor in front of the phase χ in Eq. (9c) has a relatively weak dependence on b. However, the relative phase χ of the excitation amplitudes for the $H(2p_0)$ and $H(2p_1)$ sublevels is sensitive to the collision energy. This sensitivity gives rise to the strong energy dependence of the angular momentum which, in turn, reflects the strength and the "attractive" or "repulsive" nature of the interaction potential, corresponding to positive or negative value of $\langle L_\perp \rangle$, respectively. This interpretation of our finding is in good qualitative agreement with the "rolling ball" model proposed by Hertel *et al.*[1(a)] and "propensity rule" of Andersen *et al.*[1(b)]

The alignment angle γ defined in Eq. (8a) is displayed in Fig. 9 as a function of energy and impact parameter, along with the experimental results of Hippler *et al.*[7] Again, the present results reproduce the measurement reasonably well, showing a decreasing trend of γ with increasing b. As argued above, the phase χ is relatively insensitive to impact parameter, but very sensitive to collision energy. Hence, the b dependence of the alignment angle γ is considered to be due primarily to that of the ratio of the $H(2p_0)$ and $H(2p_1)$ amplitudes in Eq. (8a). Thus, the situation here is quite similar to that described earlier for the differential A_{20}, where again only ratio of the amplitudes determines the shape of the curves.

IV. CONCLUSION

A systematic study of the $H(n=2)$ excitation process in H + He collisions in the energy regime from 0.8 to 8 keV was carried out using a molecular-orbital expansion method. The present study clearly identifies the collision dynamics of $H(n=2)$ excitation strongly suggesting the dominance of Σ-Σ radial coupling, followed flux mixing due to strong Σ-Π coupling in the $H(n=2)$ manifold for the exit channel. Calculated alignment, orientation parameters, and alignment angle are in good accord with recent measurement. Some discrepancies between the present results and the measurements are seen in the $H(2s)$ and $H(2p)$ excitation cross sections at the lower energies. Additional measurement at lower energies would be desirable.

ACKNOWLEDGMENTS

This work has been supported in part by the U.S. Department of Energy [Office of Health and Environmental Research, under Contract No. W-31-109-Eng-38, for the work of one of us (M.K.) and the Office of Basic Energy Science, Division of Chemical Sciences, for the work of the other (N.F.L.)] and by the Robert A. Welch Foundation. The authors thank Dr. R. Hippler and Dr. H. O. Lutz for useful discussions.

[1]General review in this recent progress, see, for example, (a) I. V. Hertel, H. Schmidt, A. Bähring, and E. Meyer, Rep. Prog. Phys. **48**, 375 (1985); (b) N. Andersen, J. W. Gallagher, and I. V. Hertel, in *Electronic and Atomic Collisions,* edited by D. C. Luentz, W. Meyerhof, and J. R. Peterson (North-Holland, Amsterdam, 1986), p. 57.

[2]M. Kimura and C. D. Lin (unpublished).

[3]A. Jain, C. D. Lin, and W. Fritsch, Phys. Rev. A **35**, 3180 (1987).

[4](a) M. Kimura and N. F. Lane, Phys. Rev. Lett. **56**, 2610 (1986); (b) Phys. Rev. A (to be published); (c) T. Andersen, H.-P. Neitzke, M. Kimura, and N. F. Lane, J. Phys. B **20**, 1789 (1987).

[5]See, for example, N. Andersen and S. E. Nielsen, Adv. At. Mol. Phys. **18**, 265 (1982).

[6]W. Fritsch, Phys. Rev. A **35**, 2342 (1987).

[7]R. Hippler, W. Harbich, M. Faust, H. Kleinpoppen, and H. O. Lutz, in *Abstracts of the Tenth International Conference on Atomic Physics, Tokyo, 1986,* edited by H. Narumi (North-Holland, Amsterdam, 1987).

[8]L Szasz, *Pseudopotential Theory of Atoms and Molecules* (Wiley, New York, 1985).

[9]J. Pascale, Phys. Rev. A **28**, 632 (1983).

[10]J. B. Delos, Rev. Mod. Phys. **53**, 287 (1981).

[11]M. Kimura and W. R. Thorson, Phys. Rev. A **24**, 1780 (1981).

[12](a) U. Fano, Phys. Rev. **90**, 577 (1953); (b) K. Blum and H. Kleinpoppen, Phys. Rep. **52**, 204 (1979). Using the density-matrix description, these authors gave explicit expressions for orientation vector and alignment tensor for excited states in terms of the quantities λ, χ, and σ defined in Eqs. (10a) and (10b). In these notations, orientation vector and alignment tensor are expressed by state multipoles.

[13]J. H. Birely and R. J. NcNeal, Phys. Rev. A **5**, 257 (1972).

[14]I. Sauers and E. W. Thomas, Phys. Rev. A **10**, 822 (1974).

[15]B. van Zyl and M. W. Gealy, Phys. Rev. A **35**, 3741 (1987).

[16]H. Levy, Phys. Rev. **185**, 7 (1969).

[17]F. R. Flannery and K. J. McCann, J. Phys. B **7**, 1558 (1974).

[18]M. R. Flannery, J. Phys. B **2**, 913 (1969).

[19]K. L. Bell, A. E. Kingston, and T. G. Winter, J. Phys. B **9**, L279 (1976).

[20]See, for example, C. D. Lin, Comment. At. Mol. Phys. **11**, 261 (1982).

[21]M. Kimura and N. F. Lane (unpublished).